Increasing April-May rainfall, El Niño and high vulnerability behind deadly flooding in Afghanistan, Pakistan and Iran

Authors

Mariam Zachariah, *Grantham Institute, Imperial College London, UK*
Fahad Saeed, *Climate Analytics, Berlin, Germany; Weather and Climate Services, Islamabad, Pakistan*
Clair Barnes, *Grantham Institute, Imperial College London, UK*
Ben Clarke, *Grantham Institute, Imperial College London, UK*
Maja Vahlberg, *Red Cross Red Crescent Climate Centre, the Hague, Netherlands (based in Ubmeje/Umeå, Sweden)*
Lisa Thalheimer, *United Nations University, Institute for Environment and Human Security, Bonn, Germany*
Friederike E. L Otto, *Grantham Institute, Imperial College London, UK*

Review authors

Sjoukje Philip, *Royal Netherlands Meteorological Institute (KNMI), De Bilt, The Netherlands*
Sarah Kew, *Royal Netherlands Meteorological Institute (KNMI), De Bilt, The Netherlands*
Roop Singh, *Red Cross Red Crescent Climate Centre, the Hague, Netherlands (based in New Jersey, USA)*
Luis C. Rodriguez, *International Federation of Red Cross and Red Crescent Societies, Regional Office for Asia Pacific, Kuala Lumpur, Malaysia*
Anam Zeb, *German Red Cross, Berlin, Germany (based in Islamabad, Pakistan)*
Adnan Khan, *Pakistan Red Crescent Society, Islamabad, Pakistan; Red Cross Red Crescent Climate Centre, the Hague, Netherlands*

Main findings

- Afghanistan and Pakistan are highly vulnerable to flooding due to factors such as limited transboundary water management, unplanned urban expansion, and deforestation which are contributing to increased flood risks, in combination with socio-economic conditions and compounding natural hazards, e.g. earthquakes, landslides, and drought. While Iran is less vulnerable than the other countries studied, urban infrastructure-related vulnerabilities in some cities in the northeast contributed to the impacts.

- The floods also occurred on top of existing vulnerabilities linked to complex crises. Displaced populations were particularly impacted, especially as limited essential infrastructure was destroyed and already vulnerable populations were exposed to more waterborne diseases.
- The event, despite occurring outside the usual rainy season, is not a particularly rare event in today's climate that has been warmed by 1.2°C with a return time of about ten years under the current El Niño Southern Oscillation (ENSO) conditions.

- The declining El Niño Southern Oscillation, a naturally occurring climate phenomenon, is important to explain the variability in the observed rainfall, consistent with previous research. In observations, as compared to a neutral ENSO year, the declining El Niño resulted in a consistent increase across all datasets by a factor of about two in likelihood and about 8% in intensity.

- To assess the role of human-induced climate change we combine observation-based products and climate models that include the observed ENSO relationship and assess changes in the likelihood and intensity for the heavy rainfall in the study region. While the last 40 years of observational data show an increase, climate models have a very different signal, depending on the model, with some showing an increase and some a decrease. Consequently, without further analysis into why the models show such different behaviour we can not attribute the observed increase, which is also not consistent across observation-based products, to human-induced climate change.

- The disagreement between model results and observations prevents us from concluding with certainty that human-induced climate change is the main driver making this event more likely. However, given the observed trend over the last 40 years, the absence of evidence does not mean that human-induced climate change is not a driver of increasingly heavier rainfall in this region and season in a warmer climate.

- There are ample opportunities to improve climate adaptation and resilience through, for example, investing in building resilient infrastructure and reinforcing existing structures to withstand extreme events, implementing more comprehensive nature-based solutions, increasing the coverage of early warning systems, and improving flood risk management policy and planning.

1 Introduction

Since April 2024, large parts of central Asia have been hit by a series of storms resulting in heavy downpours and multiple widespread flooding in the affected areas. These episodes were just outside of the main rainfall season in these parts from November to early April (winter months). It is worth noting that this year, the region had experienced a severe precipitation deficit from December to March, before going on to receive higher than normal precipitation and multiple flooding events in the subsequent two months that are unusual for this time of the year.

Heavy rainfall in various parts of Pakistan around April 12 affected the Khyber Pakhtunkhwa (KP) and Balochistan provinces. Following this first wave that resulted in severe losses nationwide, including 107 deaths, 130 injuries, 464 schools damaged, over 5,000 houses affected, and more than 500 livestock killed (ReliefWeb, 30 April, 2024), a second spell of heavy rains between April 28-29

disproportionately affected the Khyber Pakhtunkhwa province, with flood-related losses in multiple districts of KP (OCHA Pakistan, 30 April 2024). While provinces of KP and Balochistan received multiple westerly waves resulting in a few moderate to heavy falls, May remained excessively dry in the country overall (Pakistan Monthly Climate Summary, May 2024).

Similarly, torrential rains and river overflows on April 16 caused significant distruction in the provinces of Sistan and Baluchestan, Kerman, and Hormozgan in southeast Iran (National Council of Resistance of Iran, 18 April 2024). These floods led to power outages, isolating over 20 villages in Chabahar alone, and disrupting communications to 300 other villages in the region. In Chabahar, situated in the Sistan and Baluchestan province, river floods caused extensive damage to roads, agriculture, and urban areas, severing access to 73 villages (National Council of Resistance of Iran, 18 April 2024). One of the last storm systems of the season around May led to heavy downpours primarily over Afghanistan and Turkmenistan, and the eastern parts of Iran. Around 38 millimetres (1.5 inches) of rain fell in one hour on 15 May on Mashhad, in northeast Iran, killing seven people (Al-Monitor, 16 May 2024).

In Afghanistan, heavy rains and flash floods at the beginning of May affected the Herat and Sari Pul provinces(Xinhua, 6 May 2024). This episode had followed storms and floods earlier in April that killed more than 70 people and injured about 50 others elsewhere in Afghanistan (PBS, 13 May 2024). The last wave of storms resulted in flash floods on May 17, 2024, while the country was still reeling from the previous deluges, and impacted the provinces of Ghor, Faryab, Sari Pul, Samangan, Balkh, and Badghis (ReliefWeb, 20 May 2024).

The substantially warmer-than-usual western Indian Ocean likely played a key role in providing both dynamical and thermodynamical forcing for excessive precipitation in the region, supplemented by moisture from the warm tropical regions. El Niño is also known to influence the variability of precipitation over the region. The prevalence of El Niño during April, in tandem with a warm western Indian Ocean, points towards the possible influence of El Niño in exacerbating precipitation. Literature suggests that the warm phase of ENSO is associated with enhanced precipitation in CSWA (Central South West Asia) region in spring season especially after the mature phase of El Nino, which is in-line with the 2024 conditions which saw ENSO going into a neutral phase in May (Mariotti, 2007). Considering the scale of precipitation being much higher than average, this points towards the larger role of warm western Indian Ocean anomalies in resulting in higher April-May precipitation over the region and the role of teleconnections besides El Nino.

1.1. Event Definition

As described above, multiple storm systems brought unusual rains over Afghanistan, western Pakistan, and eastern Iran in April and May 2024, causing significant impacts. To conduct a formal attribution analysis of this event, we first define the event to reflect its spatial and temporal extent, extremeness, and the nature and extent of the impacts.

For the spatial definition of the event, we focus on a region centred on Afghanistan, along with the Iranian provinces of Razavi Khorasan, Sistan and Baluchestan, Hormozgan, Kerman, and South Khorasan in the west, and the Balochistan and KP provinces of Pakistan in the east. This area covers the flood-impacted regions through April and May 2024. Due to the atypicality of this season, occurring outside of the usual seasonal rainfall peak and featuring an unusual number of storms that

made it wetter than normal, we choose the seasonal accumulated precipitation during April and May for the temporal definition. Fig. 1 shows the total rainfall over the region during April-May 2024. The study region is highlighted in red. Fig. 2 shows the absolute seasonal anomaly wrt to 1991-2020 for the region, which was anomalously wet as a result of the multiple storms. Fig. 3 shows the annual time series of April-May seasonal accumulated rainfall area-averaged over the study region. The 2024 event is the most extreme in these datasets.

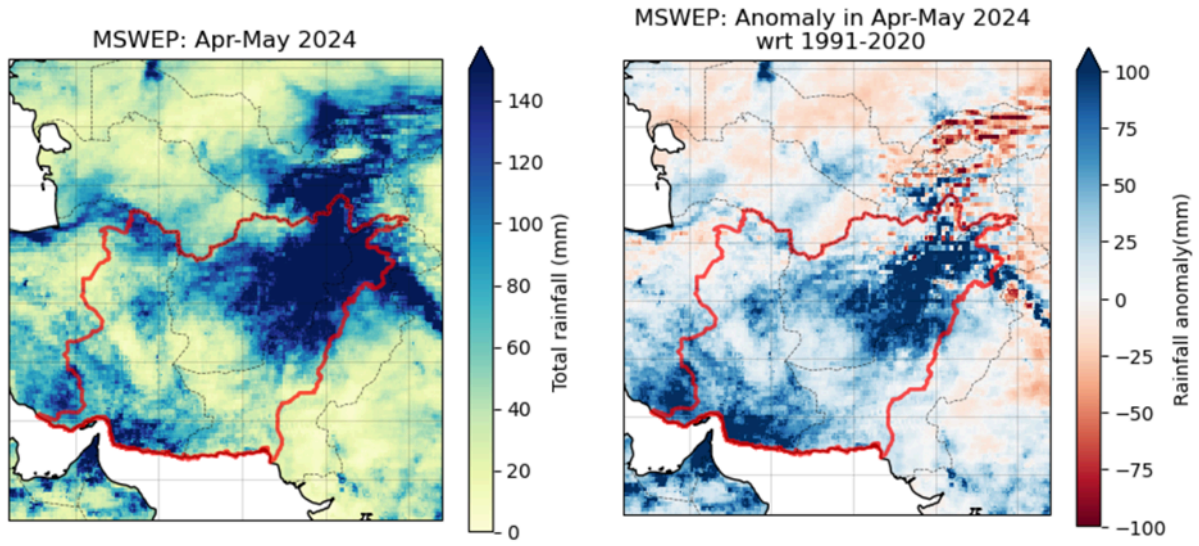

Figure 1: *(a) Observed total accumulated precipitation during April-May 2024. The red highlight shows the study region comprising the most impacted regions. (b) same as (a) showing the anomaly w.r.t 1991-2020 period. [Data source: MSWEP]*

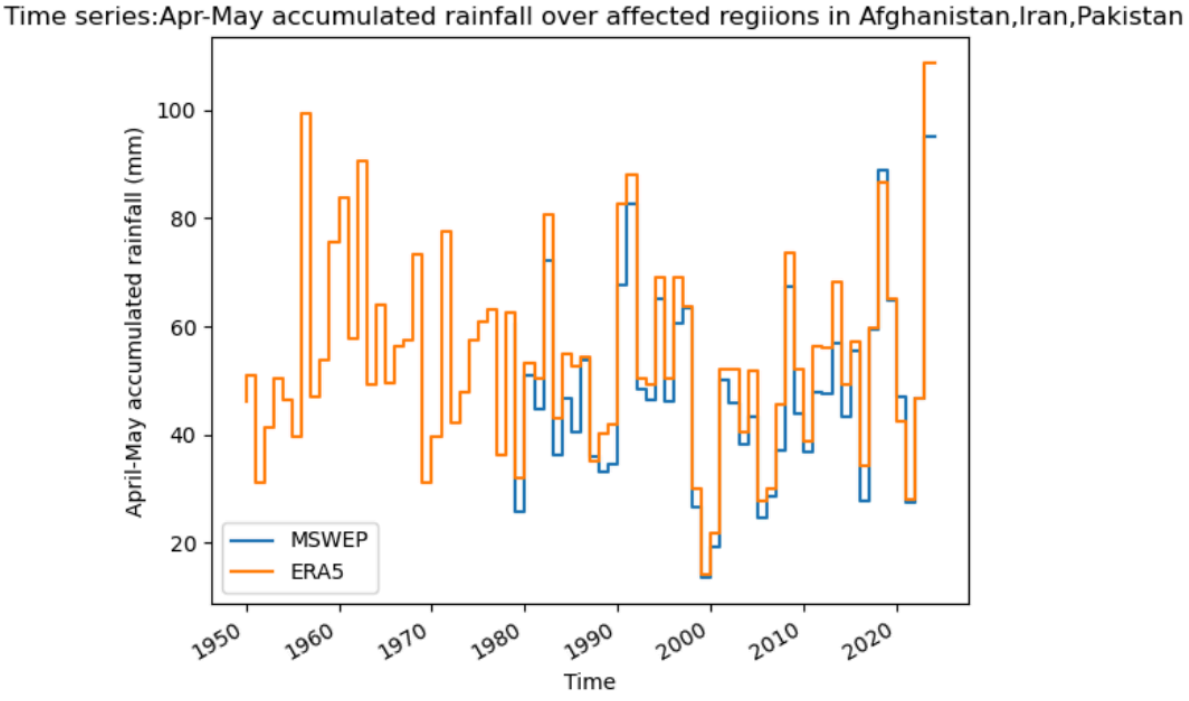

***Figure 2**: Time series of the accumulated rainfall during April-May, area-averaged over the study region based on the MSWEP and ERA5 datasets.*

Future projections of average rainfall in the region have large uncertainties and there are in general few studies finding significant changes with little consensus on the sign and with a tendency for reduction of rainfall in CMIP5 being reversed in CMIP6 across all warming levels (Gutierrez et al., 2021). However, regardless of the sign of the precipitation change in the high-mountain regions of Central Asia, the influence of the warming on the snowpack will cause important changes in the timing and amount of the spring melt (Diffenbaugh et al., 2013) with large consequences for flooding and fresh water availability. There is also strong agreement in the IPCC AR6 assessment, which includes scientific literature available up to January 2021, that heavy rainfall on short timescales of 1 to 5 days has increased in a warmer world, and is projected to increase further with future warming (Seneviratne et al., 2021), again with important consequences for flood risk. This does not necessarily mean however that also more rain is falling over longer timescales, such as the period of 2 months considered here that led to impacts in this region.

Studies focussing specifically on the affected countries are rare and show a similar uncertain picture about current and future changes in spring rainfall over Afghanistan, with increases in some regions and decreases in others, but overall no significant changes (Aich et al., 2017, Rahimi et al., 2024). Short term rainfall events on the other hand, such as RX5-day, show an increasing trend (Suryavanshi et al., 2022). For Pakistan the picture is very similar, with uncertain and highly varying trends depending on timescale and region considered when looking at total precipitation but a comparable strong increase in the most extreme precipitation (in this case the 99th percentile) especially in the Western part of the country which is also the region assessed in this study (Khan et al., 2022). In Iran across the country the short term heavy precipitation is likewise increasing (Zarrin and Dadashi-Roudbari 2021) while spring precipitation is projected to decrease in some regions while increasing in others (Doulabian et al., 2020).

2 Data and methods

2.1 Observational data

We use four gridded datasets in this study, for analysing the trends in the very wet rainfall during April and May over the study region.

1. The European Centre for Medium-Range Weather Forecasts's 5th generation reanalysis product, ERA5, is a gridded dataset that combines historical observations into global estimates using advanced modelling and data assimilation systems (Hersbach et al., 2020). This data is available from the year 1950 and at 0.5° × 0.5° from the Climate Explorer. We use precipitation data from this product.
2. The Multi-Source Weighted-Ensemble Precipitation (MSWEP) v2.8 dataset (updated from Beck et al., 2019) is fully global, available at 3-hourly intervals and at 0.1° spatial resolution, available from 1979 to ~3 hours from real-time. This product combines gauge-, satellite-, and reanalysis-based data.

3. The CRU TS (Climatic Research Unit Timeseries; Schneider et al., 2013) monthly timeseries of precipitation available for 1901-2022. The data set is gridded to 0.5x0.5 degree resolution, based on analysis of over 4000 individual weather station records. Many of the input records have been homogenized, but the data set itself is not strictly homogeneous.

As a measure of anthropogenic climate change we use the (low-pass filtered) global mean surface temperature (GMST), where GMST is taken from the National Aeronautics and Space Administration (NASA) Goddard Institute for Space Science (GISS) surface temperature analysis (GISTEMP, Hansen et al., 2010 and Lenssen et al. 2019).

As a measure of the El Niño - Southern Oscillation (ENSO) cycle we use the detrended Niño3.4 index. This is the Niño3.4 index (average SST over 5° S–5° N, 120°–170° W) minus the SST between 20° S–20° N to adjust the index for climate change, as proposed in Van Oldenborgh et al., 2021, but without rescaling each calendar month.

2.2 Model and experiment descriptions

We use 3 multi-model ensembles from climate modelling experiments using very different framings (Philip et al., 2020): Sea Surface temperature (SST) driven global circulation high resolution models, coupled global circulation models and regional climate models.

1. Coordinated Regional Climate Downscaling Experiment CORDEX-CORE over the West-Asia domain with 0.22 km resolution (WAS-22) (Teichman et al., 2021). The ensemble consists of 2 regional climate models each downscaling 4 GCMs. These simulations are composed of historical simulations up to 2005, and extended to the year 2100 using the RCP8.5 scenario.

2. CMIP6. This consists of simulations from 13 participating models with varying resolutions. For more details on CMIP6, please see Eyring et al., (2016). For all simulations, the period 1850 to 2015 is based on historical simulations, while the SSP5-8.5 scenario is used for the remainder of the 21st century.

3. HighResMIP SST-forced model ensemble (Haarsma et al. 2016), the simulations for which span from 1950 to 2050. The SST and sea ice forcings for the period 1950-2014 are obtained from the 0.25° x 0.25° Hadley Centre Global Sea Ice and Sea Surface Temperature dataset that have undergone area-weighted regridding to match the climate model resolution (see Table B). For the 'future' time period (2015-2050), SST/sea-ice data are derived from RCP8.5 (CMIP5) data, and combined with greenhouse gas forcings from SSP5-8.5 (CMIP6) simulations (see Section 3.3 of Haarsma et al. 2016 for further details).

2.3 Statistical methods

In this analysis we analyse time series from April-May accumulated precipitation for the study region over Iran, Afghanistan and Pakistan (see event definition: Figure 2), where reasonably long records of observed data are available. Methods for observational and model analysis and for model evaluation and synthesis are used according to the World Weather Attribution Protocol, described in Philip et al.

(2020), with supporting details found in van Oldenborgh et al. (2021), Ciavarella et al. (2021) and here.

The analysis steps include: (i) trend calculation from observations; (ii) model evaluation; (iii) multi-method multi-model attribution and (iv) synthesis of the attribution statement.
We calculate the return periods, Probability Ratio (PR; the factor-change in the event's probability) and change in intensity of the event under study in order to compare the climate of now and the climate of the past, defined respectively by the GMST values of now and of the preindustrial past (1850-1900, based on the Global Warming Index). To statistically model an event such as this one, we usually use a Gaussian distribution that scales with GMST. Noting from previous evidence on links between heavier precipitation in and around the study region with natural modes of variability-primarily, El Nino Southern Oscillation and the Western Tropical Indian Ocean Sea surface temperatures, among other factors (please see discussion in Section 3.1), we test four models to consider these modes of variability, in addition to the influence of GMST. Based on goodness of fit, to statistically model the event under study, we use a Gaussian distribution that scales with GMST and NINO3.4, as also discussed in Section 3.1. Details of this approach can be found in Kimutai et al. (2024) and Barnes et al. (2024). Next, results from observations and models that pass the evaluation tests are synthesised into a single attribution statement.

3 Observational analysis

3.1 Influence of modes of natural variability

During the wet season, which lasts from November to April, the ENSO has a large positive effect on precipitation variability in the CSWA area. The North Atlantic Oscillation (NAO) and El Niño Southern Oscillation (ENSO) influence winter precipitation in Central Southwest Asia, with positive NAO and warm ENSO phases leading to increased precipitation through intensified western disturbances (Syed et al., 2006). In another study, Abid et al (2020) found that ENSO influences wet season precipitation in CSWA through a combination of direct effects, involving a Rossby wave-like pattern influencing the region in the tail months, and indirect effects, through an atmospheric dipole of diabatic heating anomalies in the tropical Indian Ocean that generate persistent Rossby wave-like forcing throughout the season, with the strongest impacts occurring when both the direct and indirect effects align, crucial for hydroclimate predictability. Kamil et al. (2019) showed that over the Western Himalaya–Karakoram–Hindukush region that encompasses our study region, there is a significant increase in the correlation between the frequency of midlatitude storms that are responsible for the regional winter precipitation (December–April) and precipitation after the 1980s, highlighting the modulating influence of ENSO on storm tracks and precipitation anomalies. Mariotti (2007) showed that the warm phase of ENSO is associated with enhanced precipitation in the CSWA region in the spring season especially after the mature phase of El Nino, which is in-line with the 2024 conditions which saw ENSO going into a neutral phase in May. There are also studies that show that SST variations in the Western Indian Ocean (WIO) are correlated with precipitation anomalies in large parts of Asia including CSWA. In general, when SSTs are above average in the WIO, CSWA tends to experience wetter spring seasons. We test four statistical models for determining the best-fitting model that is representative of the observed variable distribution-

1. Model 1: $X \sim Norm(\mu, \sigma | \mu_0, \sigma_0, \alpha, T)$

2. Model 2: $X \sim Norm(\mu, \sigma | \mu_0, \sigma_0, \alpha, \beta, T, Nino)$
3. Model 3: $X \sim Norm(\mu, \sigma | \mu_0, \sigma_0, \alpha, \lambda, T, WISST)$
4. Model 4: $X \sim Norm(\mu, \sigma | \mu_0, \sigma_0, \alpha, \beta, \lambda, T, Nino, WISST)$

where X is the time series of the April-May accumulated precipitation area-averaged over the study region, T is the 4-year smoothed annual global mean surface temperature anomaly, $Nino$ is the detrended Nino3.4 index for the DJF season, $WISST$ is the detrended Western Tropical Indian Ocean sea surface temperature anomaly for Apr-May. μ_0 and σ_0 are the location and scale and parameters of the nonstationary distribution; and α, β, λ are the trends due to GMST, ENSO and the Western Tropical Indian Ocean SSTs, respectively. As a result, the location and scale of the distribution have a different value in each year, determined by both the GMST, Niño3.4 states and the Western Indian Ocean SSTs. Maximum likelihood estimation is used to estimate the model parameters, with

$$\mu = \mu_0 exp\left(\frac{\alpha T}{\mu_o}\right) \quad \text{and} \quad \sigma = \sigma_0 exp\left(\frac{\alpha T}{\mu_o}\right) \text{ for Model 1}$$

$$\mu = \mu_0 exp\left(\frac{\alpha T + \beta . Nino}{\mu_o}\right) \quad \text{and} \quad \sigma = \sigma_0 exp\left(\frac{\alpha T + \beta . Nino}{\mu_o}\right) \text{ for Model 2}$$

$$\mu = \mu_0 exp\left(\frac{\alpha T + \lambda . WISST}{\mu_o}\right) \quad \text{and} \quad \sigma = \sigma_0 exp\left(\frac{\alpha T + \lambda . WISST}{\mu_o}\right) \text{ for Model 3 and}$$

$$\mu = \mu_0 exp\left(\frac{\alpha T + \beta . Nino + \lambda . WISST}{\mu_o}\right) \quad \text{and} \quad \sigma = \sigma_0 exp\left(\frac{\alpha T + \beta . Nino + \lambda . WISST}{\mu_o}\right) \text{ for Model 4.}$$

Table 1 shows the Akaike Information Criterion values for each of the tested models for the time series from the three observed datasets identified for the study- MSWEP, ERA5 and CRU-TS. As highlighted in the table, Model 2 that accounts for the ENSO state and GMST is found to be the best-fitting model for all three datasets. Therefore, section 3.2 discusses the trends due to GMST and Nino3.4 during DJF from fitting this model to the three observed datasets.

Table 1: *Akaike Information Criterion values for the four tested models. The best-fitting model based on the lowest AIC values is highlighted in green.*

	Model 1	Model 2	Model 3	Model 4
MSWEP	396.8153	378.8029	394.1164	380.1447
ERA5	651.3454	645.2207	653.1562	647.1433
CRU-TS	516.9998	513.3576	518.4029	513.0314

3.2 Trend-fitting and Return period

Fig. 3(a-c) shows the responses of April-May seasonal precipitation over the study region to the global mean temperature (*left*) and Nino3.4 (*right*), based on the MSWEP, ERA5 and CRU-TS datasets, respectively. It should be noted that while the MSWEP and ERA5 datasets include the 2024

event, these are relatively shorter starting from 1979 and 1950, respectively. The CRU-TS dataset is longer with data since 1901, but runs only until 2022. When considering all of the data, there is no discernible trend in this variable in ERA5 (left panel, Fig. 3(b)) and a slightly decreasing trend in CRU-TS with respect to increase in GMST (left panel, Fig. 3(c)). On the contrary, the shorter MSWEP dataset shows an increasing trend with increase in GMST (left panel, Fig. 3(a)). All three datasets show an increasing response to Nino3.4- in other words, if the ENSO phase during the DJF season is positive (El Nino), the precipitation during April-May over the study region tends to be more, and progressively lesser if the ENSO phase is neutral or in the La Nina state(right panels; Fig. 3).

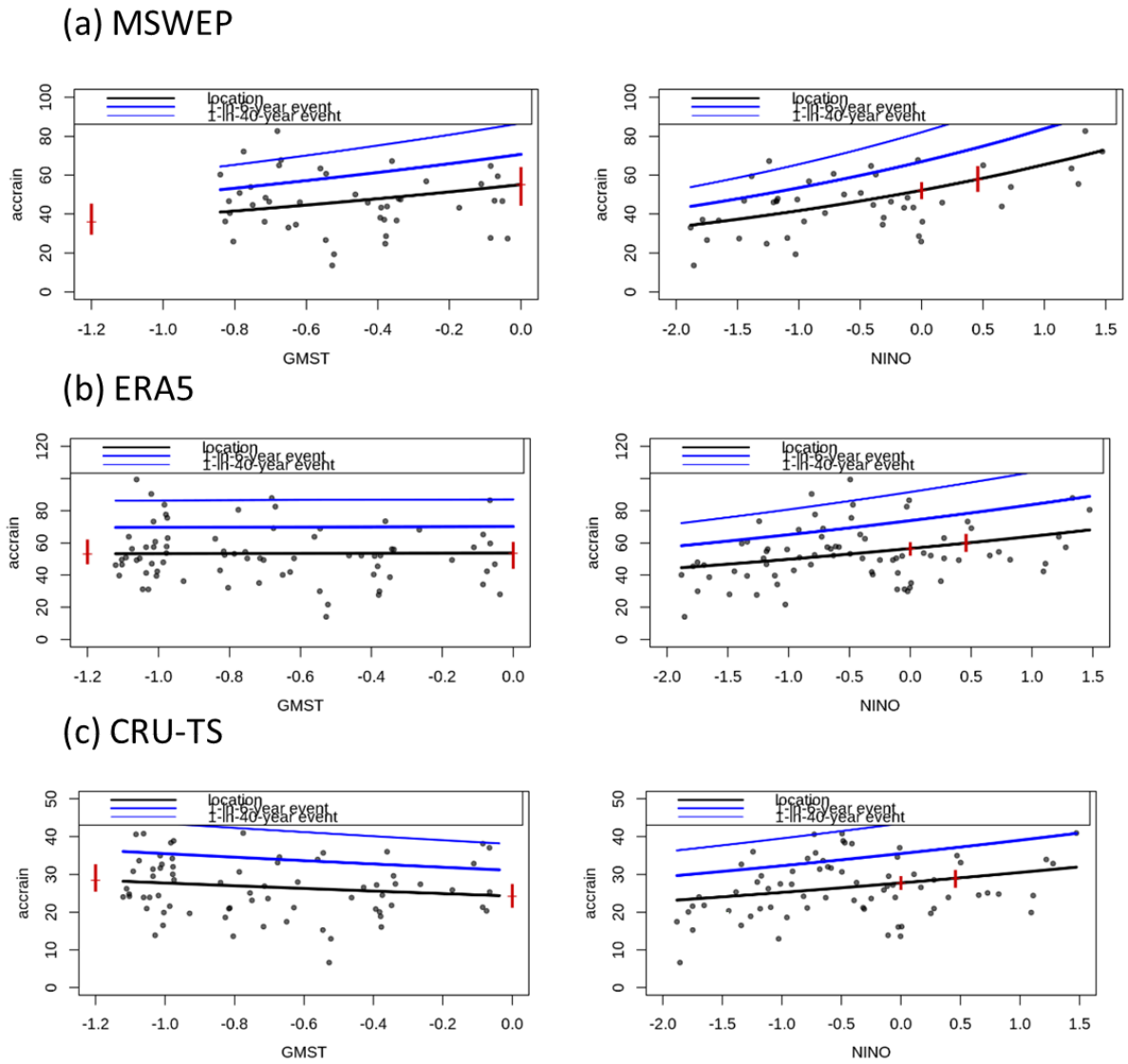

Figure 3: *Trend in April-May precipitation over the study region as a function of GMST (left) and as a function of Nino3.4 (right) for (a) MSWEP (b) ERA5 and (c) CRU-TS datasets. The thick black line denotes the location parameter of the fitted distribution, and the blue lines show estimated 6- and 40-year effective return levels for each year.*

Fig. 4(a-c) shows the return period curves for the 2024 climate and a 1.2 °C cooler climate based on the MSWEP, ERA5 and CRU-TS datasets. The 2024 event has a return period of 11 years (uncertainty: 4 - 1136 years) in the MSWEP dataset. The event is rare in the longer ERA5 dataset with a return period of 180 years (uncertainty: 24 -516743 years). At the time of this study, we do not have

access to the station data to validate the reliability of the data before the satellite-era (before 1980). Therefore, we define the event as a 1-in-10 year event (based on MSWEP) for the remainder of the analysis.

The best estimates for probability ratio between the present 2024 climate vs. 1.2 °C cooler climate centres on no change in the ERA5 and CRU-TS datasets, but with large uncertainty (1.2 for ERA5 (uncertainty: 0 to 150) and 1 for CRU-TS (uncertainty: 0.2 to 3)), along with best estimates for intensity change of 1.8% and 0.9% increase in rainfall amounts as compared to an event of the same rarity as the observed event, respectively, albeit with large uncertainties (30% decrease to 30% increase in both datasets). In the MSWEP dataset, the event is around 1664 times more likely (uncertainty: 0.5 to 4.67E+07) and 53% wetter (uncertainty: 4% drier to 109% wetter) now compared to the 1.2 °C cooler climate of the past.

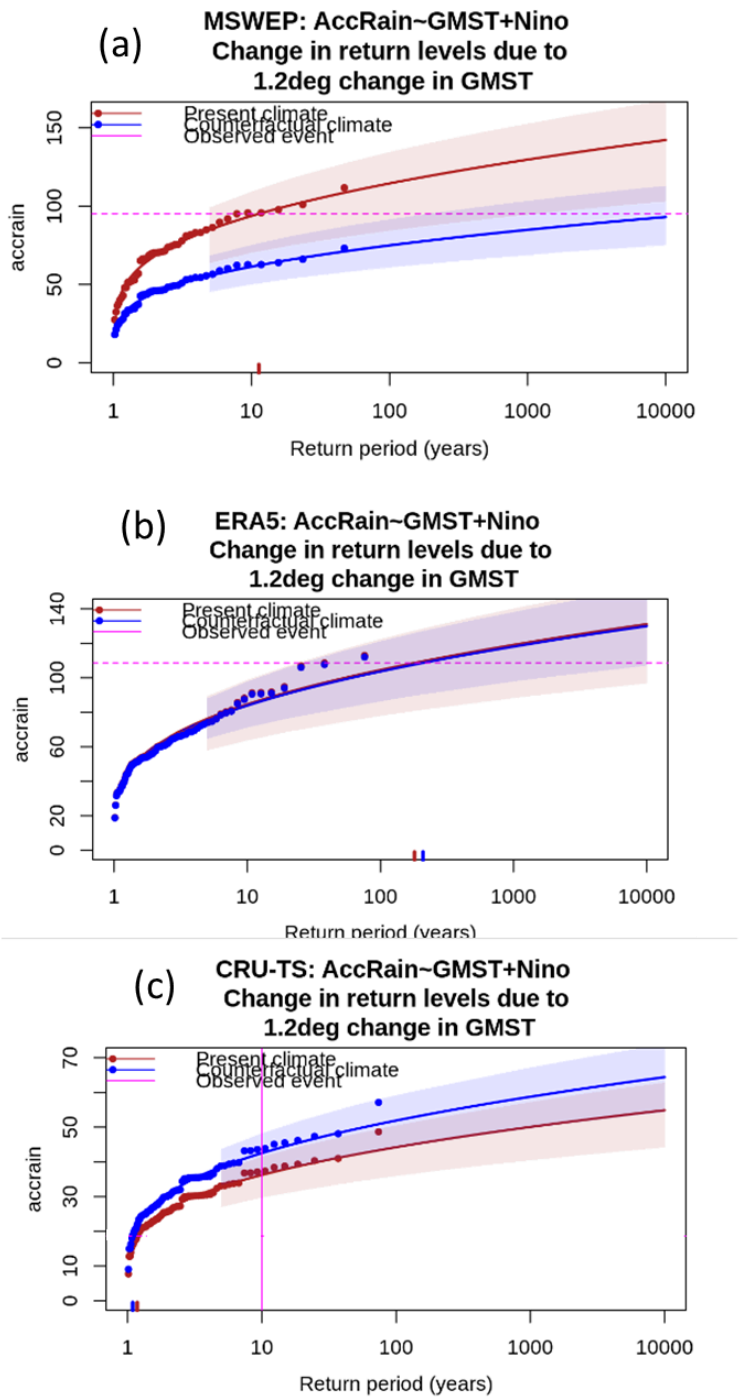

Figure 4: *Gaussian fit with fixed dispersion, and location parameter scaling proportional to GMST of the index series.* ***(a)*** *Return time plots for the climate of 2024 (red) and a climate with GMST 1.2 ºC cooler (blue), based on MSWEP observations. The past observations are shown twice: once shifted up to the current climate and once shifted down to the climate of the pre-industrial era. The markers show the data and the lines show the fits and uncertainty from the bootstrap. The magenta line shows the magnitude of the 2023/24 event analysed here.* ***(b)*** *same as (a) for ERA5 dataset,* ***(c)*** *same as (a) for CRU-TS dataset. Given that the event is not in the CRU-TS dataset, the vertical magenta line goes through the return period of 10 years, to highlight the change in intensity of such an event due to climate change.*

For testing whether this difference in trends between the three datasets is an artefact of the length of data, we repeated the analysis with the data from the year 1979, for the ERA5 and CRU-TS datasets. shows the return period curves, for the 2024 climate and a 1.2 °C cooler climate for the recent 45 years for ERA5 (42 years for CRU-TS). Fig. 5(a-c) shows the return period curves based on the data from the recent ~40 years for these datasets. Consistent with MSWEP, there is a stronger increasing trend in April-May accumulated rainfall due to increase in GMST in this period in both ERA5 and MSWEP datasets. The best estimates for Probability Ratio are 360 (uncertainty: 0.013 to 8.15E+06)) and 71 (uncertainty: 0.7 ro 1.9E+07)) for ERA5 and CRU-TS , respectively, with intensity changes of 36% (uncertainty: 17% drier to 90% wetter) and 33% (4% drier to 84% wetter), respectively.

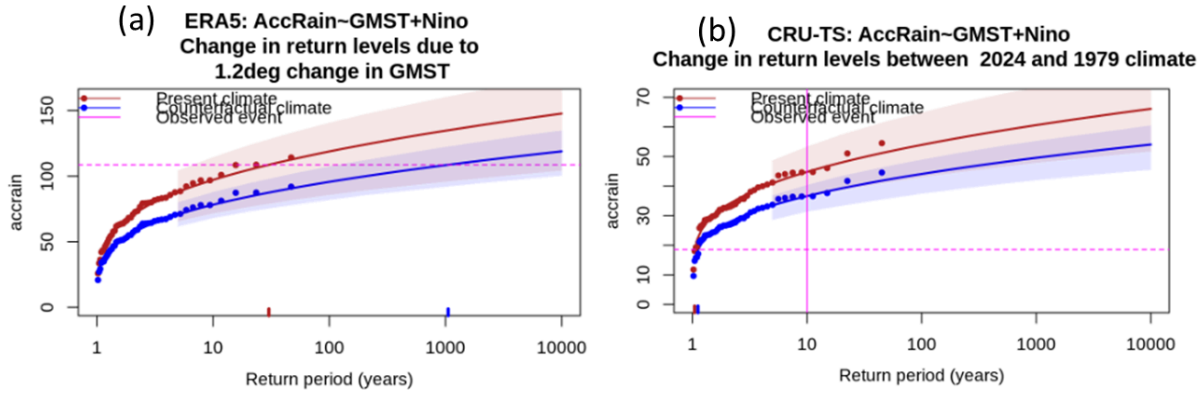

Figure 5: *Same as Figure 4, but with data from 1979 to 2024.*

The non-availability of long and quality-controlled station-based observations in the rapid timeframe of this study renders it difficult to explain the increase in trends in the last~40 years (and the lack thereof in the longer datasets) in the context of anthropogenic climate change; however, the agreement between the datasets in the last 40 years (Fig. 6) unequivocally points to an increasing trend in precipitation with increase in GMST. The event has probability ratios of 66 (0.6 to 4000), 35(0.3 to 3570) and 13(0.8 to5000) in the 2024 climate as compared to the 1979 climate, and 35% (-2.5% to 68%), 24% (-12% to57%) and 22% (-3% to 54%) wetter.

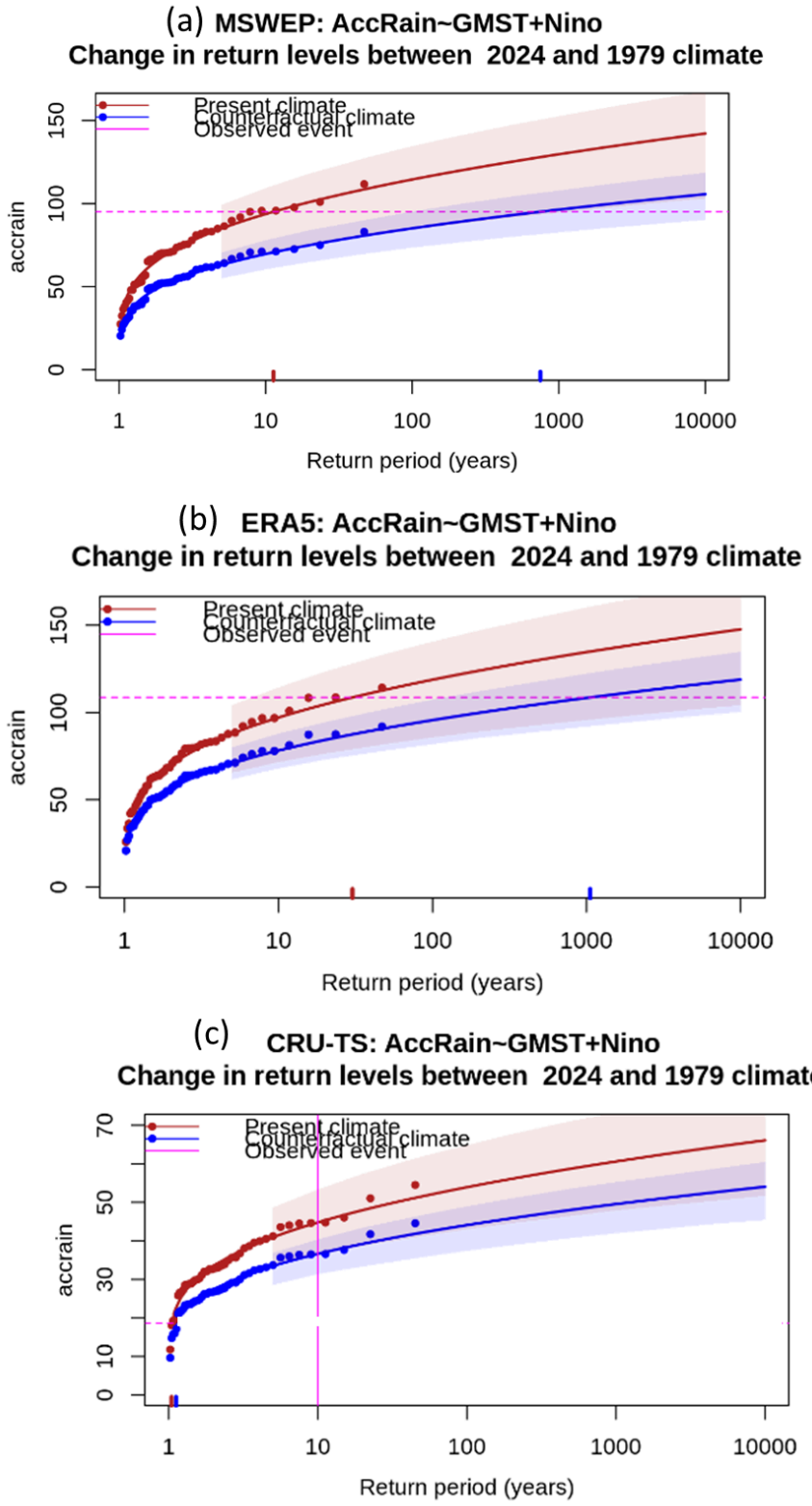

Figure 6: *Same as Figure 4, showing the return period plots for the 2024 climate and the 1979 climate, and demonstrating the trend over the last ~40 years.*

4 Model evaluation

In this section we show the results of the model evaluation for the study region over Afghanistan, Iran and Pakistan (see Fig.1). The climate models are evaluated against the observations in their ability to capture:

1. Seasonal cycles: For this, we qualitatively compare the seasonal cycles based on model outputs against observations-based cycles. We discard the models that exhibit multi-modality and/or ill-defined peaks in their seasonal cycles.

2. Spatial patterns: Models that do not match the observations in terms of the large-scale precipitation patterns during April-May are excluded.

3. Parameters of the fitted Gaussian Models (dispersion parameter). We discard the model if the model and observation parameter ranges do not overlap.

4. Correlation between April-May seasonal precipitation and the detrended Niño3.4 index. We discard the model if the model and observation parameter ranges do not overlap.

The models are labelled as 'good', 'reasonable', or 'bad' based on their performances in terms of the three criteria discussed above. We evaluate 9 models from HighResMIP, 5 models from CORDEX and 14 models from CMIP6, as listed in Table 2.

Table 2: *Evaluation results of the climate models considered for attribution analysis of April-May accumulated precipitation over the region. For each model, the expected temperature of a 1-in-10 -year event is shown, along with the best estimate of the Sigma and Shape parameters and a 95% confidence interval for each, obtained via bootstrapping. Based on overall suitability, the models are classified as good, reasonable or bad, shown by green, yellow and red highlights, respectively.*

Model / Observations	**Seasonal cycle**	**Spatial pattern**	**Dispersion**	**Correlation with Nino3.4**	**Event magnitude (mm)**
MSWEP			0.291 (0.229 ... 0.342)	0.54 (0.30 ... 0.57)	95.09
ERA5			0.318 (0.261 ... 0.362)	0.31 (0.090 ... 0.47)	108.64
CRUTS			0.273 (0.232 ... 0.305)	0.28 (0.10 ... 0.44)	does not have the event.
					Threshold for 1-in-10 year event (mm)
HighResMIP					
CMCC-CM2-HR4	bad	good	0.450 (0.346 ... 0.507)	0.24 (0.0073 ... 0.45)	89.77
CMCC-CM2-VHR4	bad	good	0.391 (0.305 ... 0.439)	0.012 (-0.20 ... 0.24)	114.21
EC-Earth3P-HR	good	good	0.356 (0.277 ... 0.401)	0.31 (0.12 ... 0.49)	66.20
EC-Earth3P	reasonable	good	0.401 (0.301 ... 0.462)	0.32 (0.17 ... 0.46)	76.32
HadGEM3-GC31-HM	good	good	0.371 (0.298 ... 0.424)	0.25 (0.063 ... 0.42)	59.88

HadGEM3-GC31-LM	bad	reasonable	0.522 (0.383 ... 0.593)	0.49 (0.32 ... 0.65)	102.92
HadGEM3-GC31-MM	bad	good	0.466 (0.366 ... 0.535)	0.30 (0.12 ... 0.46)	81.75
MPI-ESM1-2-HR	good	good	0.593 (0.466 ... 0.673)	0.023 (-0.19 ... 0.25)	80.26
MPI-ESM1-2-XR	reasonable	good	0.712 (0.458 ... 0.819)	-0.0062 (-0.22 ... 0.20)	54.17
CORDEX			(...)	(...)	
MIROC5_rcp85_r1i1p1_RegCM4-7	bad	good	0.329 (0.247 ... 0.386)	0.32 (0.11 ... 0.50)	168.60
MPI-ESM-LR_rcp85_r1i1p1_COSMO-crCLIM-v1-1	reasonable	reasonable	0.389 (0.303 ... 0.444)	0.34 (0.18 ... 0.49)	70.99
MPI-ESM-MR_rcp85_r1i1p1_RegCM4-7	bad	good	0.323 (0.262 ... 0.362)	0.14 (-0.091 ... 0.34)	91.07
NorESM1-M_rcp85_r1i1p1_COSMO-crCLIM-v1-1	reasonable	reasonable	0.319 (0.238 ... 0.369)	0.34 (0.15 ... 0.51)	93.98
NorESM1-M_rcp85_r1i1p1_RegCM4-7	bad	good	0.281 (0.220 ... 0.320)	0.23 (0.025 ... 0.40)	172.37
CMIP6					
ACCESS-CM2	good	reasonable	0.367 (0.276 ... 0.431)	0.40 (0.27 ... 0.52)	94.89
ACCESS-ESM1-5	bad	bad	0.292 (0.225 ... 0.331)	0.36 (0.24 ... 0.47)	155.89
CanESM5	reasonable	reasonable	0.600 (0.470 ... 0.705)	0.54 (0.42 ... 0.65)	51.93
CMCC-ESM2	reasonable	reasonable	0.427 (0.320 ... 0.516)	0.37 (0.24 ... 0.47)	123.54
EC-Earth3	reasonable	good	0.411 (0.303 ... 0.477)	0.39 (0.26 ... 0.52)	92.77
EC-Earth3-Veg	reasonable	good	0.330 (0.266 ... 0.374)	0.43 (0.29 ... 0.55)	80.14
EC-Earth3-Veg-LR	reasonable	good	0.389 (0.291 ... 0.445)	0.40 (0.29 ... 0.50)	101.92
IPSL-CM6A-LR	good	reasonable	0.408 (0.323 ... 0.466)	0.079 (-0.075 ... 0.24)	125.18
KACE-1-0-G	good	reasonable	0.502 (0.386 ... 0.578)	0.43 (0.31 ... 0.54)	92.06
MIROC6	reasonable	bad	0.234 (0.173 ... 0.274)	0.10 (-0.057 ... 0.25)	131.83
MRI-ESM2-0	reasonable	reasonable	0.379 (0.288 ... 0.426)	0.23 (0.10 ... 0.36)	173.59
NorESM2-LM	bad	reasonable	0.390 (0.316 ... 0.444)	0.50 (0.40 ... 0.60)	99.61
NorESM2-MM	reasonable	reasonable	0.316 (0.249 ... 0.354)	0.52 (0.42 ... 0.62)	110.67

5 Multi-method multi-model attribution

Table 3 lists the probability ratios (PR) and relative changes in intensity (ΔI) based on the observations and those models that passed the evaluation described in Section 4, for a moderately extreme 10-year event, between the current climate and a pre-industrial (1.2degC cooler climate).

Table 4 shows the probability ratios and the intensity changes, but between a Nino year having the same Nino3.4 as the observed 2023/24 Nino year vs. a neutral Nino year with Nino3.4 value of 0.

Table 3: *Probability ratio and change in intensity for 10-year April-May precipitation over the study region for each model that passed evaluation: (a) from the preindustrial climate to the present and (b) from the present to 2°C above pre industrial temperatures.*

	(a) -1.2C vs present		(b) Present vs +0.8C	
Model / Observations	**Probability ratio PR [-]**	**Change in intensity ΔI [%]**	**Probability ratio PR [-]**	**Change in intensity ΔI [%]**
MSWEP	1.7e+3 (0.45 ... 4.6e+7)	53 (-3.6 ... 1.1e+2)		
ERA5	1.2 (0.00034 ... 1.5e+2)	1.8 (-28 ... 31)		
CRUTS	0.98 (0.19 ... 3.0)	0.90 (-28 ... 30)		
EC-Earth3P-HR	0.44 (0.15 ... 8.4)	-14 (-40 ... 25)	1.8 (0.86 ... 2.9)	9.9 (-2.2 ... 19)
EC-Earth3P	0.99 (0.17 ... 1.1e+2)	-0.18 (-38 ... 50)	1.5 (0.55 ... 3.0)	7.2 (-8.5 ... 21)
HadGEM3-GC31-HM	0.15 (0.12 ... 0.30)	-43 (-59 ... -21)	0.89 (0.37 ... 1.7)	-1.7 (-14 ... 8.2)
MPI-ESM-LR_rcp85_r1i1p1_COSMO-crCLIM-v1-1	0.58 (0.21 ... 6.1)	-8.4 (-30 ... 20)	0.35 (0.13 ... 0.70)	-13 (-23 ... -4.5)
NorESM1-M_rcp85_r1i1p1_COSMO-crCLIM-v1-1	0.36 (0.16 ... 1.5)	-15 (-35 ... 4.6)	0.15 (0.049 ... 0.37)	-19 (-28 ... -10)
ACCESS-CM2	1.2 (0.44 ... 6.7)	2.1 (-13 ... 23)	0.63 (0.28 ... 1.2)	-6.3 (-16 ... 3.0)
CMCC-ESM2	1.4 (0.39 ... 14)	5.1 (-18 ... 33)	0.42 (0.13 ... 0.81)	-13 (-26 ... -3.2)
EC-Earth3	0.55 (0.24 ... 2.6)	-11 (-32 ... 14)	0.29 (0.13 ... 0.61)	-18 (-28 ... -7.7)
EC-Earth3-Veg	0.27 (0.18 ... 0.74)	-28 (-42 ... -4.8)	0.26 (0.11 ... 0.61)	-19 (-30 ... -7.1)
EC-Earth3-Veg-LR	0.25 (0.15 ... 0.86)	-28 (-45 ... -2.2)	0.18 (0.039 ... 0.50)	-22 (-36 ... -9.6)
IPSL-CM6A-LR	1.2 (0.38 ... 11)	2.9 (-18 ... 28)	0.64 (0.23 ... 1.2)	-6.7 (-19 ... 2.9)
MRI-ESM2-0	0.93 (0.31 ... 5.1)	-0.91 (-18 ... 18)	1.1 (0.61 ... 1.8)	1.5 (-5.7 ... 7.6)
NorESM2-MM	6.7 (0.85 ... 2.8e+2)	20 (-2.2 ... 45)	1.4 (0.77 ... 2.2)	4.1 (-3.0 ... 11)

Table 4: *Probability ratio and change in intensity for 10-year April-May precipitation over the study region for each model that passed evaluation: (a) from the preindustrial climate to the present and (b) from the present to 2°C above pre industrial temperatures.*

	2023/24 El-Nino year vs a neutral Nino year	
Model / Observations	**Probability ratio PR [-]**	**Change in intensity ΔI [%]**
MSWEP	2.9 (1.9 ... 8.7)	11 (5.8 ... 15)

ERA5	3.0 (1.5 ... 8.0)	6.0 (1.5 ... 9.9)
CRUTS	1.4 (1.1 ... 1.9)	3.5 (0.83 ... 6.1)
EC-Earth3P-HR	3.3 (1.4 ... 18)	16 (4.5 ... 31)
EC-Earth3P	5.4 (2.0 ... 28)	22 (9.2 ... 37)
HadGEM3-GC31-HM	1.5 (0.74 ... 4.3)	5.3 (-4.5 ... 18)
MPI-ESM-LR_rcp85_r1i1p1_COSMO-crCLIM-v1-1	2.9 (1.0 ... 18)	13 (0.42 ... 30)
NorESM1-M_rcp85_r1i1p1_COSMO-crCLIM-v1-1	4.4 (1.8 ... 17)	16 (6.7 ... 26)
ACCESS-CM2	1.6 (0.84 ... 4.1)	6.3 (-2.7 ... 17)
CMCC-ESM2	2.7 (1.4 ... 8.9)	14 (5.0 ... 27)
EC-Earth3	8.8 (2.5 ... 50)	30 (15 ... 44)
EC-Earth3-Veg	27 (6.3 ... 5.8e+2)	40 (25 ... 60)
EC-Earth3-Veg-LR	2.8e+2 (55 ... 3.2e+3)	56 (43 ... 71)
IPSL-CM6A-LR	2.2 (1.0 ... 7.1)	11 (0.47 ... 23)
MRI-ESM2-0	3.7 (1.8 ... 9.8)	14 (7.0 ... 23)
NorESM2-MM	5.3 (2.1 ... 27)	17 (8.2 ... 30)

6 Hazard synthesis

For the event definition described above we evaluate the influence of anthropogenic climate change on the event by calculating the probability ratio as well as the change in intensity using observation-based products and climate models. Models which do not pass the evaluation described above are excluded from the analysis. The aim is to synthesise results from models that pass the evaluation along with the observations-based products, to give an overarching attribution statement. Fig. 7 shows the changes in probability and intensity for the observations (blue) and models (red) and Fig. 8 shows the same, but only using observations since the beginning of the satellite era (1979). Before combining them into a synthesised assessment, first, a representation error is added (in quadrature) to the observations, to account for the difference between observations-based datasets that cannot be explained by natural variability. This is shown in these figures as white boxes around the light blue bars. The dark blue bar shows the average over the observation-based products. Next, a term to account for intermodel spread is added (in quadrature) to the natural variability of the models. This is shown in the figures as white boxes around the light red bars. The dark red bar shows the model average, consisting of a weighted mean using the (uncorrelated) uncertainties due to natural variability plus the term representing intermodel spread (i.e., the inverse square of the white bars). Observation-based products and models are combined into a single result in two ways. Firstly, we neglect common model uncertainties beyond the intermodel spread that is depicted by the model average, and compute the weighted average of models (dark red bar) and observations (dark blue bar): this is indicated by the magenta bar. As, due to common model uncertainties, model uncertainty can be larger than the intermodel spread, secondly, we also show the estimate of an unweighted, direct average of observations (dark red bar) and models (dark blue bar) contributing 50% each, indicated by the white box around the magenta bar in the synthesis figures. As especially when only considering the last 40 years observations show a strong increase in the event considered, while models overall

show a decrease the weighted and unweighted means are qualitatively and quantitatively very different. The synthesised results are not qualitatively different when only considering the last 40 years of observations that show a trend in all datasets. While the trend across the observed datasets is not statistically significant, the best estimate changes are large compared to increasing rainfall on other timescales and in other regions (e.g., Brazil, the UK or South Africa) with a best estimate PR of about 350 and an intensity increase of 40% compared to a 1.2°C cooler climate. Furthermore, considering the global warming between 1979 and today with the world having warmed approximately by 0.84degC, the 2024 event is 31 times more likely (uncertainty: 1.77 to 550) and 27% wetter (uncertainty: 6.44% to 44.7%) compared to the 1979 climate.

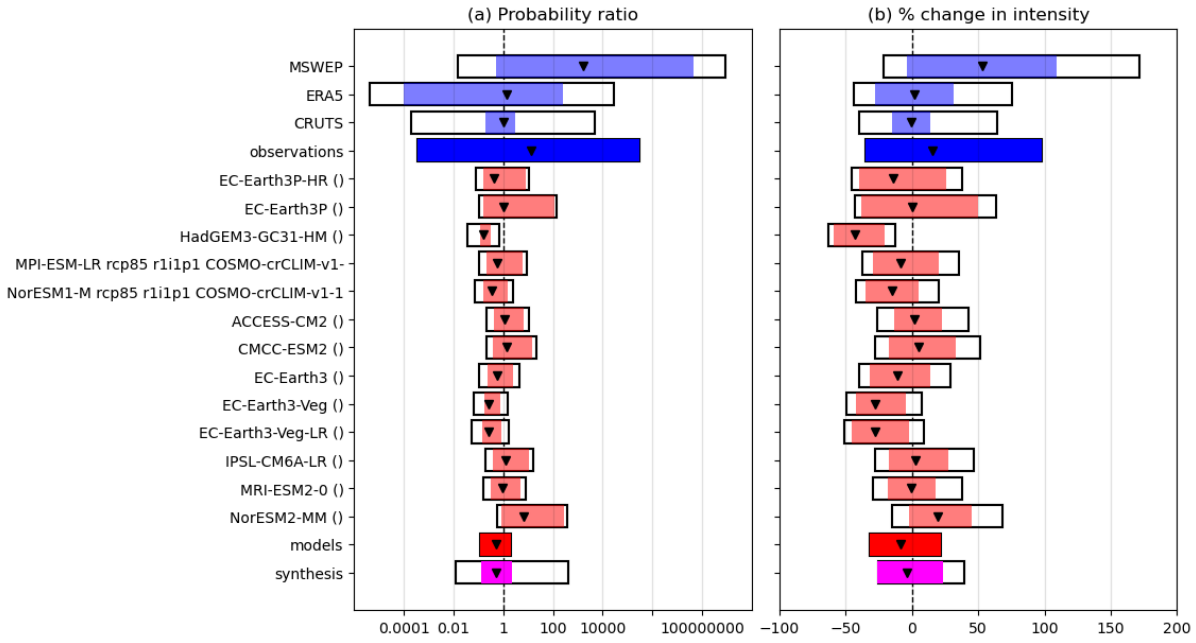

Figure 7: *Synthesis of (a) change in intensity and (b) probability of a one-in-10-year April-May season over the study region between a 1.2°C cooler preindustrial climate and the 2024 climate, for all models that were judged 'reasonable' or 'good' in the model evaluation step and using all available observational data. Details of how to interpret the synthesis plots are given in the text.*

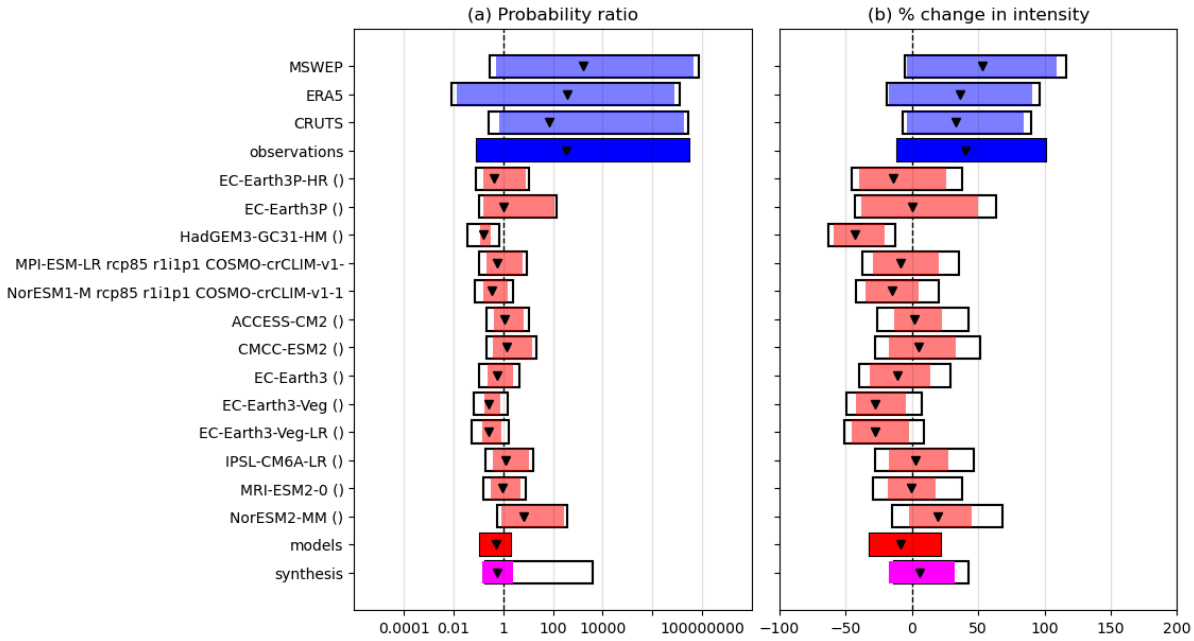

Figure 8 *as Figure XX, but with trends in the observational datasets (blue bars) estimated using only observational data from 1979 onwards, showing the stronger trend over this period. Note that the estimated changes in the observations are shown only for comparison with Figure XX, to highlight the difference in trend over the shorter time period; the estimated values are therefore not expected to accurately represent the actual change in intensity or likelihood in similar events with respect to a 1.2C cooler climate.*

The model results are very different in individual models, with some showing an increase and some a decrease. Lacking a clear physical reason of why climate change should lead to a decrease or an increase of 2-month precipitation in the April-May season, we cannot exclude models on the basis of the trend from the analysis. Thus, we do not provide a quantitative assessment of the attribution analysis but note that all the observational datasets tested show a strong trend in the last 40 years, that is only represented in few models and thus cannot be attributed to human-induced climate change. We also highlight, though, that there is also no known driver of a trend other than human-induced climate change that could explain the observed trend. For any planning purposes it is thus important to treat this absence of evidence from the models not as evidence for a small role of climate change in explaining the observed trend over the last 40 years, but on the contrary, given that this could be a climate change driven trend, that it could get even stronger with continued burning of fossil fuels.

In contrast to the role of climate change, models and observation based-products agree quantitatively and qualitatively on the role of the DJF El Nino in increasing the likelihood and intensity of this event (Fig. 9). For the observations, the probability ratio is 4.65 (0.417-53), and the change in intensity is 6.72% (-1.41% to 15.3%). The probability ratio and intensity changes from the models are 2.3 (0.870- 7.43) and 19.3% (-2.42% to 45.9%), respectively. We thus communicate the numbers as a doubling in likelihood (PR= 2.58 (1.05- 7.44)) and an increase in intensity of about 8% (deltaI=8.29% (0.6% to 16.4%).

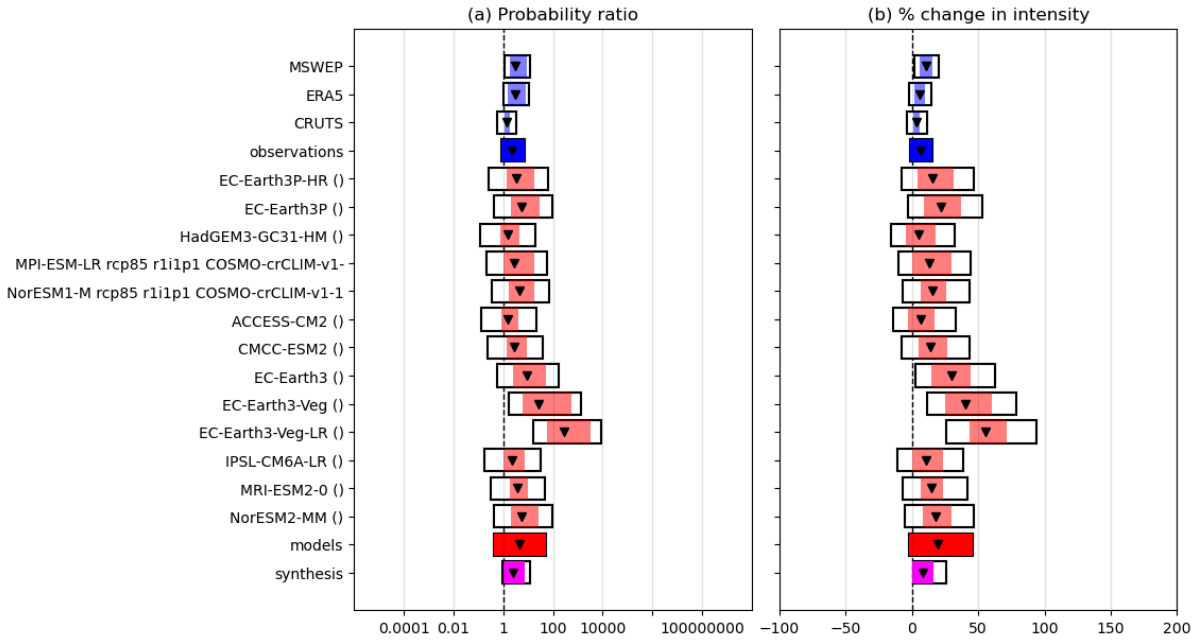

Figure 9: *Synthesis of (a) change in intensity and (b) probability of a one-in-10-year April-May season over the study region when following a year with neutral Niño conditions vs the 2023-24 El Niño event, for all models that were judged 'reasonable' or 'good' in the model evaluation step and using all available observational data. Details of how to interpret the synthesis plots are given in the text.*

7 Vulnerability and exposure

While there are significant differences between Afghanistan, Pakistan, and Iran, the provinces of the respective countries included in the spatial domain of the study are highly vulnerable to floods, due to their geographical locations and socio-economic conditions. An assessment of flood risk (as a product of hazard, exposure, vulnerability, and coping capacity) in these countries is crucial for learning from the disaster and effective flood risk management going forward.

Scoring 0,780 at the Human Development Index, Iran exhibits a higher level of development compared to Pakistan and Afghanistan and Pakistan (0.540 and 0.462, respectively) (UNDP, 2022). This is, in part, explained by better healthcare infrastructure, educational attainment, and a more diversified economy (UNDP, 2022). However, despite development gains across all three countries, recurring floods and compounding hazards erode infrastructure and disrupt socio-economic stability. In Afghanistan, provinces located near major river basins exhibit the highest flood risk, with notable vulnerability in provinces like Nimroz, Helmand, Jawzjan, and Kunduz (Ikram et al., 2024). Similarly, in Pakistan, the densely populated Indus River basin, and its transboundary tributary Kabul and Kunar rivers, face significant flood risk. In Iran, major cities situated along rivers flowing into the Persian Gulf, such as Tehran, Isfahan, and Shiraz, are vulnerable to floods.

Vulnerabilities intersect along socio-economic and demographic lines, with women, children, and marginalized communities disproportionately affected by floods. Further, studies reveal that factors like socio-economic status, housing construction material, and past flood experiences significantly influence household vulnerability (Shah et al., 2020).

The impact of these floods is compounded by other natural hazards such as landslides and droughts. The frequency and intensity of these events, some of which were exacerbated by human-induced climate change (Otto et al., 2023), pose significant challenges to disaster response and recovery efforts. Conflict-related large-scale displacement (IDMC, 2021; IDMC, 2024) further exacerbates vulnerabilities, with displaced populations often settling in flood-prone areas with inadequate infrastructure (Noori, 2024; Taraky et al., 2021). Floods also have health-related impacts as flood water serves as ideal breeding grounds for pathogens that result in diarrhea and other waterborne infections.

In light of these challenges, effective flood risk management strategies must integrate multi-dimensional approaches that address vulnerabilities, enhance infrastructure resilience, and promote sustainable practices. By understanding the complex interplay of socio-economic factors, environmental dynamics, and compounding events, policymakers can develop targeted interventions to mitigate flood risk and build resilient communities in Afghanistan, Pakistan, and Iran. Many such interventions have been identified and developed over the years, however funding remains an obstacle for implementation.

7.1 Transboundary water management

Limited transboundary water management between Afghanistan, Pakistan, and Iran is a driver of increased flood risk. Issues primarily arise from inadequate cooperation, insufficient data sharing, unilateral flood mitigation measures, and upstream development activities.

The lack of effective transboundary water agreements between Afghanistan and Pakistan hinders coordinated flood risk management efforts. Both countries share at least nine rivers, including the Kabul River, yet there are no formal agreements on joint management (Thomas et al., 2016). Insufficient data sharing and joint monitoring make it difficult to implement Early Warning Systems (EWS) and prepare for floods and droughts; hazards at the opposite ends of water-related extremes that both frequent the studied area (Taraky et al., 2021).

Unilateral flood mitigation measures also exacerbate the problem. Due to the lack of basin-wide cooperation, countries have to resort to costly and insufficient unilateral measures. For example, Pakistan and Afghanistan have undertaken independent flood mitigation projects along shared rivers, which are often inadequate for managing large-scale floods (Taraky et al., 2021). Upstream development activities in Afghanistan further complicate the situation. Afghanistan's construction of dams and expansion of agricultural activities on the Helmand River have reduced water flows into Iran, impacting the Hamun wetlands and increasing flood risks downstream (Climate Diplomacy, n.d.). Iran faces significant challenges due to diminished water flow into the Hamun wetlands, located in the Helmand/Hirmand River Basin shared by Iran and Afghanistan, which exacerbates flood risks and leads to biodiversity loss, land degradation, and displacement of local communities (reportedly 30% of the Sistan-Baluchestan population) (Maleki et al., 2019; Daryani, 2018). In addition, Pakistan is concerned about Afghanistan's potential future dam construction on shared rivers like the Kabul, which could alter water flows and increase flood risks in Pakistan (Climate Diplomacy, n.d.).

The strained relationship between Iran and Afghanistan over the Helmand River basin also highlights the risks of inadequate transboundary water management. Despite a 1973 treaty aimed at allocating water shares, the agreement has been criticized as inadequate and has never been fully implemented (Climate Diplomacy, n.d.).

Addressing these challenges requires integrated and cooperative transboundary water management strategies. The case of the Kabul River Basin demonstrates that collaborative efforts in flood risk management can yield significant socio-economic benefits for both Afghanistan and Pakistan (Taraky et al., 2021). Adopting equitable water resource utilization, and developing specific agreements as well as comprehensive flood hazard models for shared basins could help mitigate flood risks and promote regional stability and development (Allafta & Opp, 2021).

7.2 Urban development

Across the countries, flood risk is largely concentrated in urban areas, characterized by unplanned expansion, inadequate infrastructure, and poor drainage systems. In Iran, the expansion of paved surfaces associated with rapid urbanization exacerbates flood risks by reducing water infiltration (Arabameri et al., 2019). Urban areas like Mashhad, which is bearing the brunt of the 2024 floods, also suffer from deteriorated infrastructure and the destruction of natural landscapes such as waterways, both of which leading to higher flood risk (Darabi et al., 2020). Inefficient maintenance and blockage of drainage systems further contribute to flooding, where sediment accumulation hampers drainage capacity (Allafta & Opp, 2021).

In Afghanistan, particularly in Kabul, urban expansion has led to a dramatic increase in impervious surfaces - from 7.1% to 58.57% between 1960 and 2009 - significantly reducing green spaces and increasing runoff volumes, which results in frequent flooding (Manawi et al., 2020). Additionally, Kabul's flood resilience is compromised by limited community awareness, insufficient institutional support, and a lack of a comprehensive flood management policy (Mushwani et al., 2024).

Pakistan faces similar challenges, where urban planning is often reactive and short-term, focusing on constructing dikes and levees rather than implementing integrated flood risk management strategies (Rana et al., 2020). The rapid, unplanned urbanization leads to inadequate drainage systems, which are unable to handle heavy rains, causing urban flooding (Zia et al., 2023). Encroachment on natural waterways and the reduction of green infrastructure further exacerbate flood risk, as these areas lose their natural capacity to absorb excess water (Arshad et al., 2022). The neglect of topographical consideration in urban planning also places low-lying areas at heightened risk (Waseem et al., 2023).

Overall, the interplay between rapid urbanization, poor planning, and inadequate infrastructure significantly heightens flood risks in these regions, necessitating comprehensive urban planning and effective flood management policies.

7.3 Deforestation

Land use management in Iran, Afghanistan, and Pakistan significantly contributes to increased flood risk through agricultural expansion, deforestation, and inadequate water management practices.

In Afghanistan, between 1990 and 2005, the country lost a third of its trees, largely driven by conflict and illegal logging as part of the "war economy" (Bodetti, 2019). By 2013, half of Afghanistan's forests had vanished (Ibid.), with the largest tree losses recorded in the provinces of Kunar, Paktya, and Nangarhar (World Rainforests, n.d.). Since 2011, the deforestation rate has declined, without any reported tree loss during 2015 and 2017, which subsequently increased yet remained at a 20-year low (Ibid.). Pakistan faces one of the highest deforestation rates in Asia, with up to 0.5% annually and only 5.7% of its land under forest cover (Iqbal, 2019; Shahid, 2020). Deforestation in Pakistan, especially in Khyber Pakhtunkhwa, is driven by dependence on forests for fuelwood and timber, exacerbated by unemployment, poverty, and population growth (Tariq & Aziz, 2015; Mehmood et al., 2018). Ineffective forest management, illegal logging, and unregulated grazing further worsen the issue, compounded by weather-related disasters and a lack of alternative resources and awareness among local communities (WWF Pakistan, n.d.; Tariq & Aziz, 2015; Mehmood et al., 2018). In Iran, deforestation, driven by factors such as agricultural expansion, urban development, overgrazing and forest fires (Katiraie, 2019; Bodetti, 2019), resulted in the loss of over 45,000 hectares between 2020 and 2022, accounting for 70% of the deforestation rate in the past five years (IOD, 2023). Loss of forest cover reduces the land's water absorption capacity and exacerbates soil erosion (see e.g. Hajian et al., 2019), while agricultural expansion reduces natural water retention (see e.g. Sugianto et al., 2022), increasing the volume and velocity of surface runoff during times of heavy rainfall.

Reforestation efforts in Afghanistan are focused on reducing dependency on wood and provide alternative livelihoods including subsidized fuel-efficient stoves and replanted pistachio forests (Pikulicka- Wilczewska, 2019). In Iran, the One Billion Tree Planting Project was launched with a 2.27 trillion rials (about $4.5 million USD) budget to plant 300 million trees until 2025 (Tehran Times, 2023). While updates on progress are yet to be published, the project sends a clear signal that the government is prioritizing the issue of deforestation. Similarly, in Pakistan, notably the Khyber-Pakhtunkhwa province, reforestation efforts are ambitious. Its Billion Tree Tsunami project, launched in 2014, exceeded its target by planting 1.06 billion trees, meanwhile generating thousands of jobs (Prisco, 2018). Building on the project's success, the federal government launched the 10 Billion Tree Tsunami, through which another billion trees have been planted to date, in addition to creating about 84,000 daily wagers benefiting from the project (Root, 2021; Hess, 2021).

Effective reforestation initiatives and land use management are crucial to mitigate flood risks and enhance environmental resilience in these countries.

7.4 Disaster risk management

7.4.1 Flood protection

Flood protection efforts in Afghanistan, Pakistan, and Iran have evolved throughout the past decades, reflecting both the challenges and progress each country has faced in addressing flood risks.

In Afghanistan, the International Organization for Migration (IOM) has constructed flood protection walls in Nangarhar and Kunar provinces, safeguarding thousands of homes and agricultural lands. These projects were part of a broader disaster risk reduction strategy that included training local communities in emergency response and flood management (IOM, 2013; IOM, 2015). Similarly, the

World Bank supported the construction of a flood wall in Kabul Province, which has become a model for flood management across the country (World Bank, 2019). Collaborative efforts involving the IOM and Afghanistan's National Disaster Management Authority have been crucial in building local capacities for flood risk management. Additionally, the United Nations Development Programme (UNDP) and the Asian Development Bank (ADB) have contributed through community- based approaches and structural measures, respectively, to enhance flood resilience (UNDP, n.d.; ADB, 2008). The private sector has also played a role, with companies such as Guru Krupa Wires providing essential flood protection materials including gabions and wire mesh, commonly used for constructing flood barriers as well as reinforcing riverbanks (Guru Krupa Wires, n.d.).

In Pakistan, flood protection primarily involves structural solutions such as embankments, dikes, and diversion channels, which are part of the National Flood Protection Plan (NFPP-IV) for 2015-2025 (Government of Pakistan, n.d.). Despite their high cost, research suggests that these measures offer significant returns on investment. For instance, upgrading Pakistan's flood protection system could yield $11.90 in avoided damages for every dollar spent (WRI, 2023; Aqueduct Floods, n.d.). Specific initiatives, like the rebuilding of flood protection walls in Dera Ismail Khan, have effectively used local materials and community involvement to ensure durability and cost-effectiveness (Anum, 2023). A recent $77 million USD project focused on building Pakistan’s resilience to climate change through Ecosystem-based Adaptation (EbA) and Green Infrastructure for integrated flood risk management has been launched with support of the GCF (2023).

In Iran, flood management has been addressed through projects like the project HoWaMan - Flood Risk Management in Semi-Arid and Arid Areas, which evaluated current practices and highlighted the need for better administrative coordination and hazard mapping (Mohajeri, n.d.). Technical studies have emphasized the modernization of Iran's flood protection infrastructure to ensure sustainability and resilience (Fadaeifard et al., 2022). Further, the need to integrate health considerations into flood management plans has been highlighted due to the significant health impacts of floods (Sharifi & Bokaie, 2019). Advanced modeling techniques are also advocated to enhance predictive capabilities and preparedness for future floods (Zainudini & Sardarzaei, 2022).

7.4.2 Risk awareness and community coping capacity

Risk perception is crucial for the adoption of risk mitigating behavior, while playing a vital role in flood risk management and communication (Rana et al., 2020). While there is limited research on risk awareness in Afghanistan, a study by Mushwani et al. (2024) indicates that 31.3% of Kabul City residents have engaged in flood preparedness activities. Albeit limited in scope, this highlights a growing awareness and proactive stance towards flood risk.

In Pakistan, past flood experiences and proximity to hazards significantly shape risk perception, which, in turn, motivates risk mitigating behavior (Rana et al., 2020). Research shows that flood risk perception is influenced by socioeconomic factors such as age, education, house ownership, family size, past experiences, and proximity to rivers (Shah et al., 2022). Institutional factors like access to credit and weather forecasts also play a role. Notably, 51.47% of individuals with 1-10 years of education, 52.83% of those over 40 years old, and 73.02% of lower-income groups perceive high flood risk (Shah et al., 2022). Spatial differences in risk perception are evident, with inadequate public

protection measures and limited private mitigation actions contributing to high risk and lower mitigation in flash flood-prone areas (Ahmad & Afzal, 2022).

In Iran, social capital significantly impacts community resilience, with bonding capital enhancing resilience capacity. Important social criteria include respect for neighbors' rights, public green spaces, playgrounds, and tree planting (Panahandeh Khan et al., 2023). However, the overall risk perception in Iran is low, with many residents inadequately prepared for disasters, leading to higher damages and losses (Heidari et al., 2020). The Shiraz flood incident exemplifies this, where prior warnings were reportedly largely ignored and not used to inform actions such as evacuation, resulting in significant casualties (Heidari et al., 2020).

Understanding and improving flood risk perception in these regions requires addressing institutional, socioeconomic, and social factors, thereby enhancing community coping capacities and resilience.

7.4.3 Early warning systems

Flood early warning systems (EWS) play a pivotal role in mitigating the impacts of floods. In Iran, while the Iran Meteorological Organization has monitoring and warning capacity, and early warnings were issued for the 2024 floods, failure to heed these warnings and mobilise appropriate response mechanisms highlights significant gaps in Iran's flood preparedness (Etemad, 2024). Other recent flood incidents, such as the 2019 Shiraz floods, also underscore the deficiencies in the existing EWS (Heidari et al., 2020). Despite meteorological warnings issued, the lack of coordination among response organisations and human resource constraints within the Incident Command System structure hindered effective disaster response (Dizaji et al., 2019). Furthermore, low risk perception among local authorities exacerbated the vulnerability of flood-affected regions (Heidari et al., 2020).

In Pakistan, efforts have been made to enhance disaster management capabilities, including the development of a multi-hazard early warning system (MHEWS) as part of the national disaster management plan (NDMA, 2012). However, challenges persist regarding the clarity and effectiveness of delivery systems for early warnings (Ali & Iqbal, 2021). Despite improvements reported in the Sindh Resilience project, the flash nature of floods and limitations in warning dissemination continue to pose challenges (World Bank, 2021).

Afghanistan faces similar challenges with its relatively weak EWS, characterised by short lead times and deficiencies in data integration and dissemination (Morshed et al., 2024). WMO (n.d.) suggests that the Afghanistan Meteorological Department (AMD) currently lacks the necessary capacity for effective data analysis and dissemination. While province-scale flood warnings are issued, they often fail to translate into actionable measures at the local level (Manandhar et al., 2023).

To address these shortcomings, concerted efforts are required to improve coordination among stakeholders, enhance data quality and accessibility, and increase community engagement. Further, investing in technology and capacity building initiatives is essential for strengthening EWS and reducing vulnerability to floods in Iran, Pakistan, and Afghanistan.

V&E conclusions

Afghanistan, Pakistan, and Iran are highly vulnerable to flooding due to their geographical locations and socio-economic conditions. Floods exacerbated existing vulnerabilities and deepens the complex crises by displacing populations, destroying essential infrastructure and increasing the prevalence of waterborne diseases. In particular, limited transboundary water management, unplanned urban expansion, and deforestation are contributing to increased flood risks in the three countries. Limited coverage of early warning systems have resulted in varying levels of preparedness and response within the countries and within exposed groups. There are actions to address flood risk through investments in infrastructure and Nature-based Solutions in each of the three countries. However, there are ample opportunities to improve climate adaptation and resilience through, for example, investing in building resilient infrastructure and reinforcing existing structures to withstand extreme events, implementing more comprehensive nature-based solutions, increasing the coverage of early warning systems, and improving flood risk management policy and planning.

Data availability

Almost all data are or will soon be made available via the Climate Explorer.

References

All references are given as hyperlinks in the text.